

## Supplementary Material

# Pressure-Induced Enhancement of Proton Conduction across MOF Grain Boundaries

Manni Li, Dongyang Han, Lei Wu, Yian Shi, Kun Zhang<sup>†</sup>

Automotive Engineering Research Institute, Jiangsu University, Zhenjiang, Jiangsu  
212013, People's Republic of China

These authors contributed equally to this work.

<sup>†</sup>Corresponding authors.

E-mail addresses: kunzhang@ujs.edu.cn



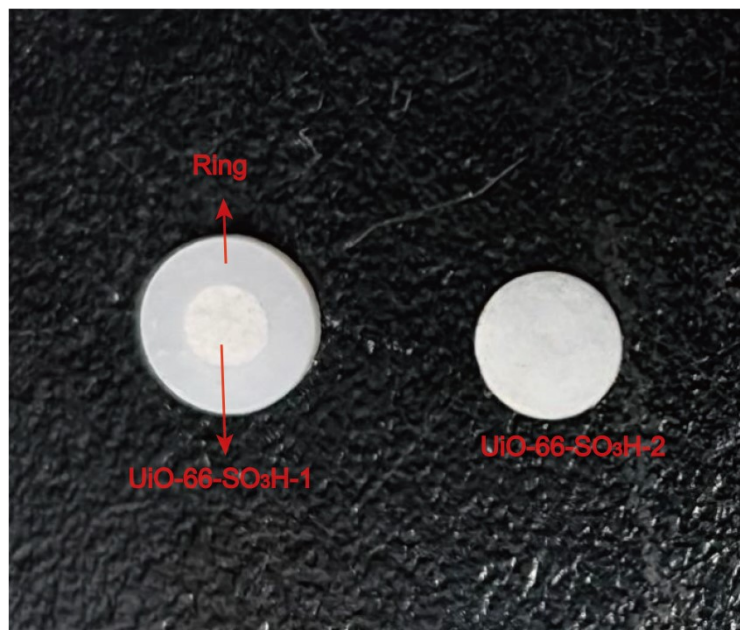


**Fig. S1.** Left: UiO-66-SO<sub>3</sub>H-1 sample; Right: UiO-66-SO<sub>3</sub>H-2 sample.

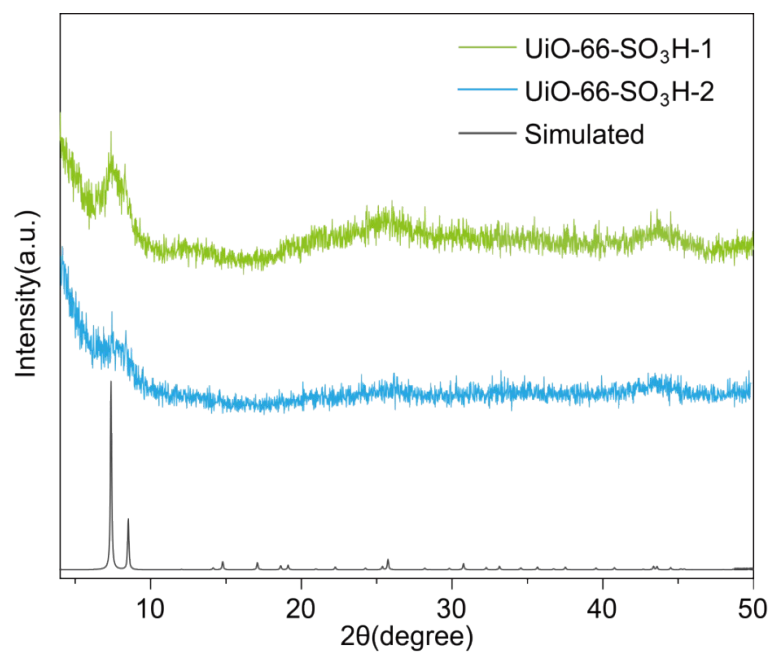


**Fig. S2.** PXRD of UiO-66-SO<sub>3</sub>H-1 and UiO-66-SO<sub>3</sub>H-2.

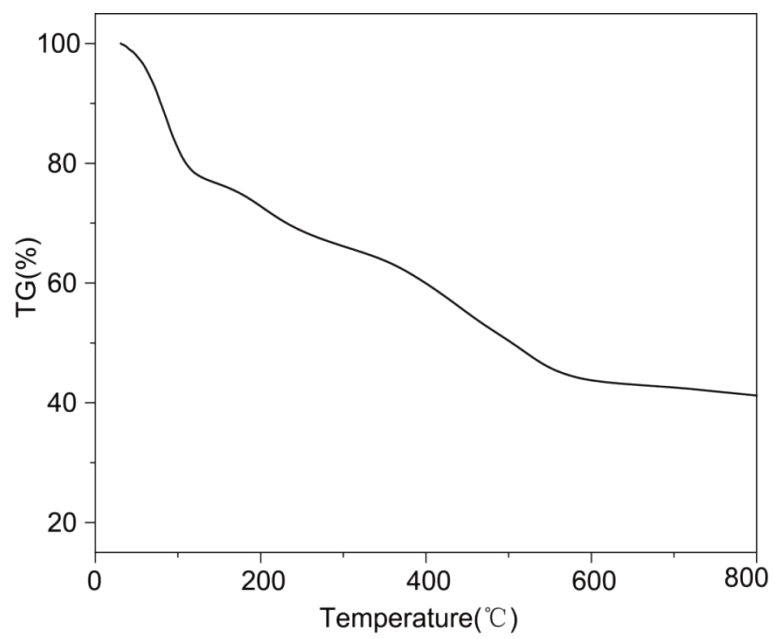


**Fig. S3.** TG of UiO-66-SO<sub>3</sub>H.

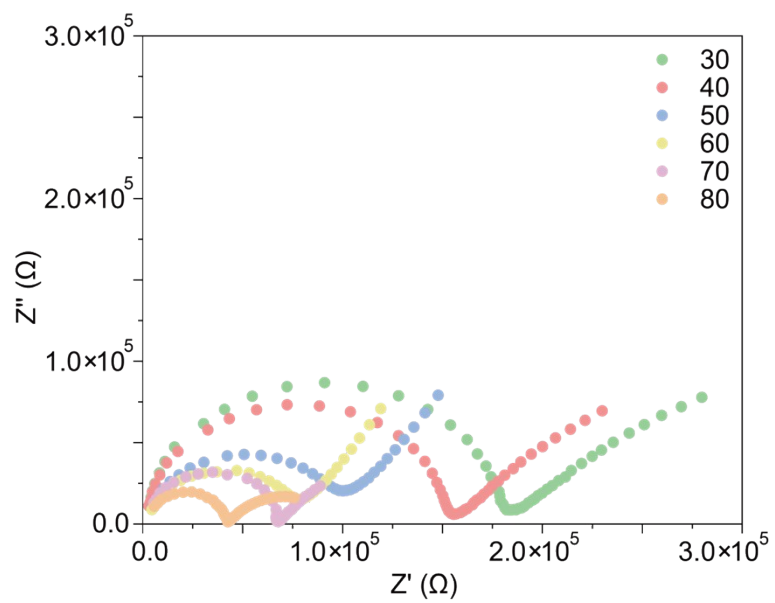


**Fig. S4.** Nyquist plot for UiO-66-SO<sub>3</sub>H-1 at 100% RH versus different temperatures.

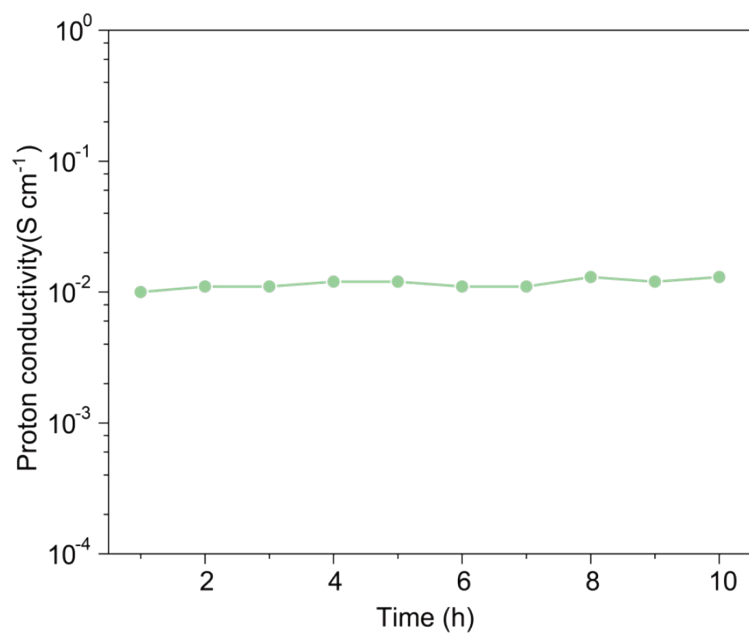


**Fig. S5.** Proton conductivity of UiO-66-SO<sub>3</sub>H-2 versus time at 80 °C and 100% RH.

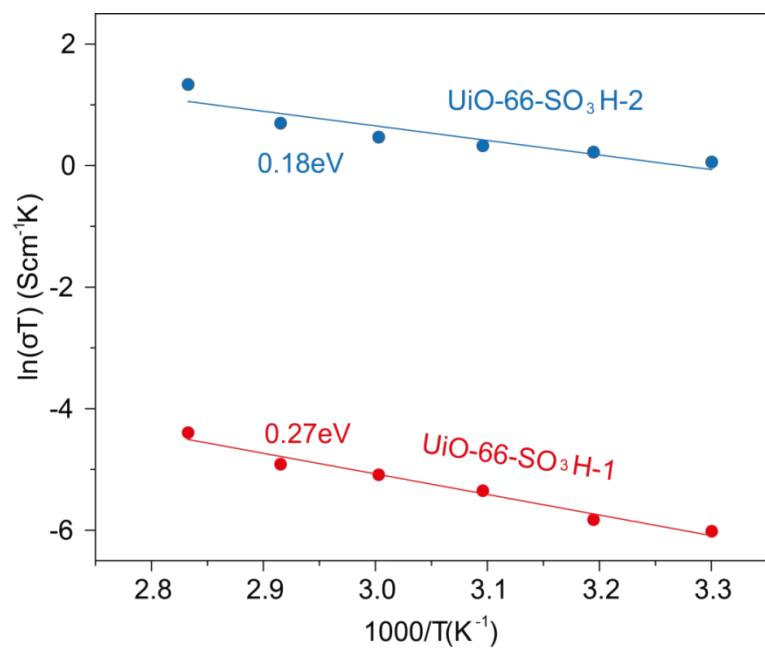


**Fig. S6.** Arrhenius plots of proton conductivity for UiO-66-SO<sub>3</sub>H-1 and UiO-66-SO<sub>3</sub>H-2.

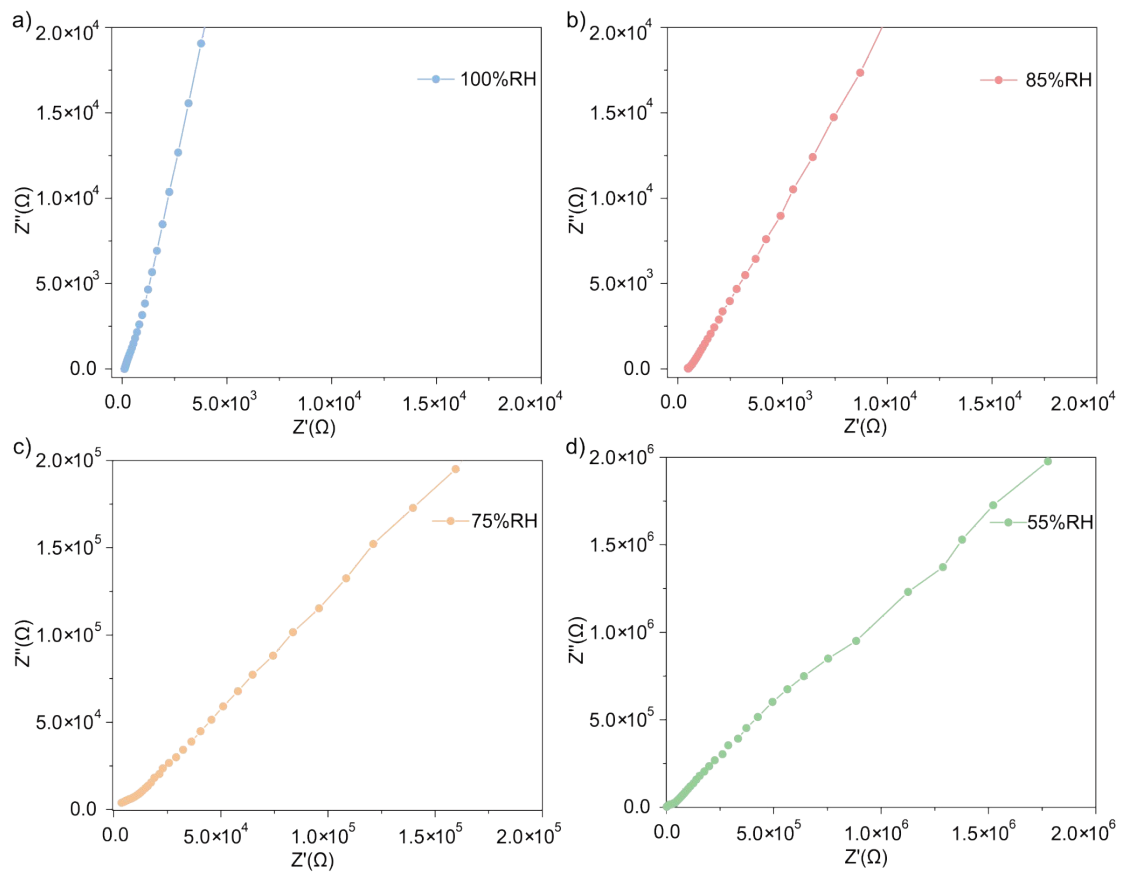


**Fig. S7.** Nyquist plot for UiO-66-SO<sub>3</sub>H-2 at 30°C versus different RHs.

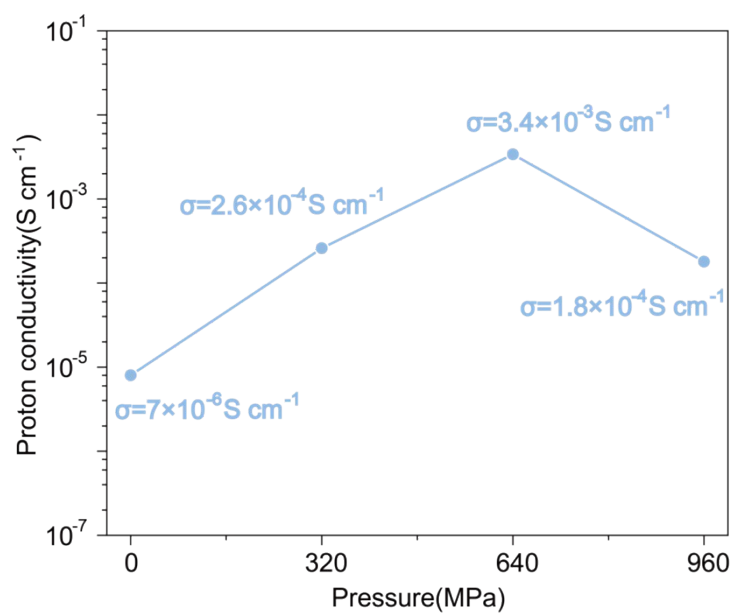


**Fig. S8.** Proton conductivity of UiO-66-SO<sub>3</sub>H pellets as a function of applied pressure.

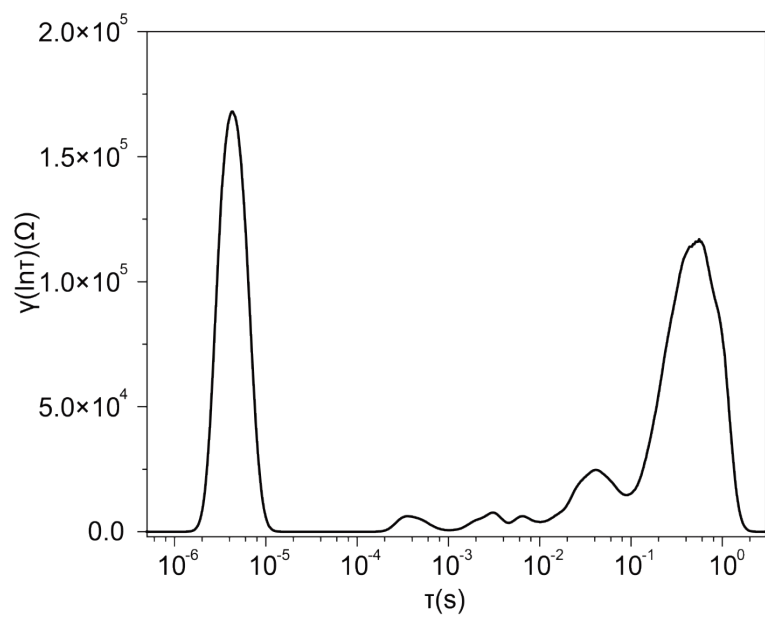


**Fig. S9.** DRT diagram of UiO-66-SO<sub>3</sub>H-1 at 40°C.

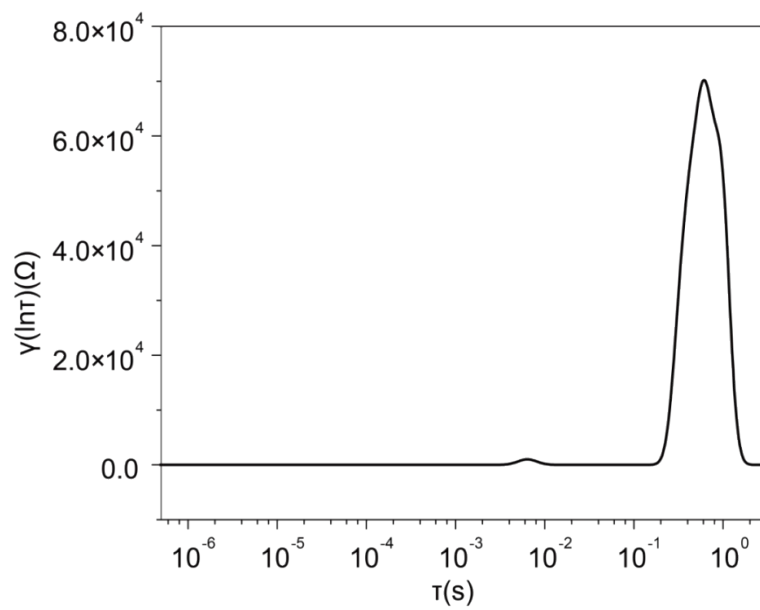


**Fig. S10.** DRT diagram of UiO-66-SO<sub>3</sub>H-2 at 40°C.

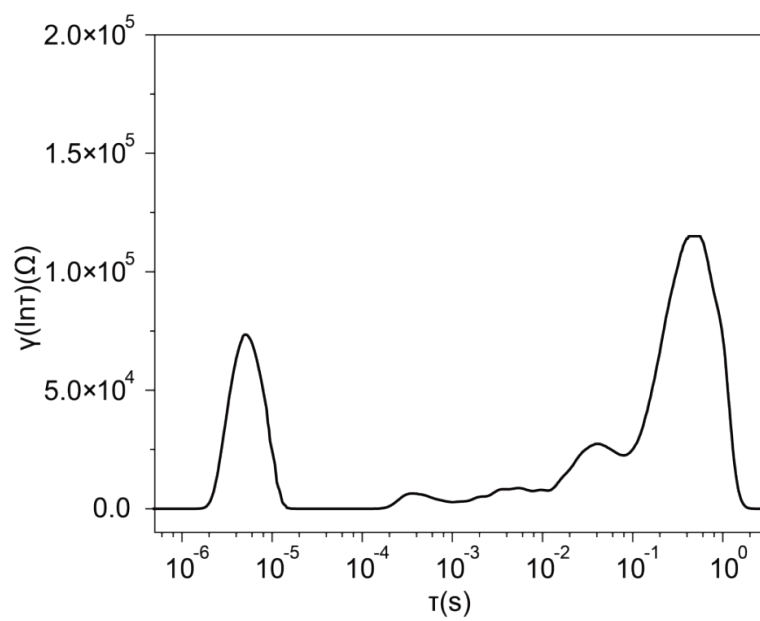


**Fig. S11.** DRT diagram of UiO-66-SO<sub>3</sub>H-1 at 50°C.

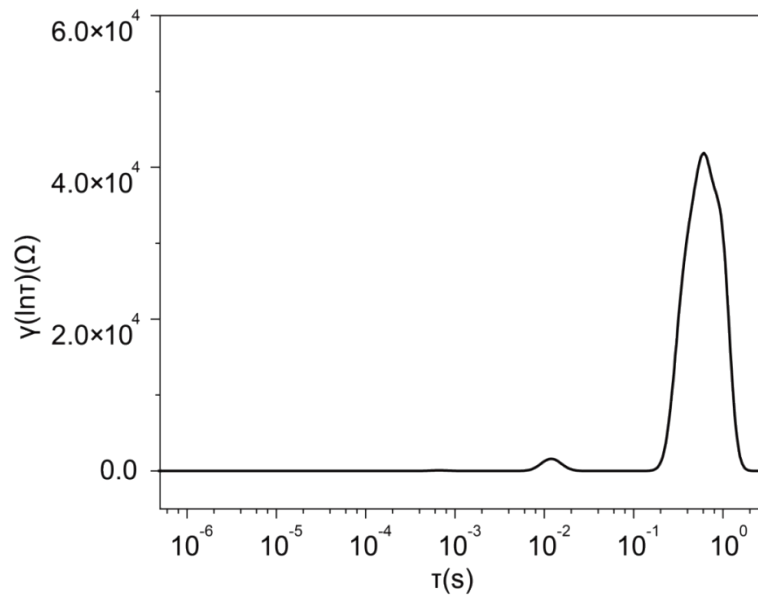


**Fig. S12.** DRT diagram of UiO-66-SO<sub>3</sub>H-2 at 50°C.

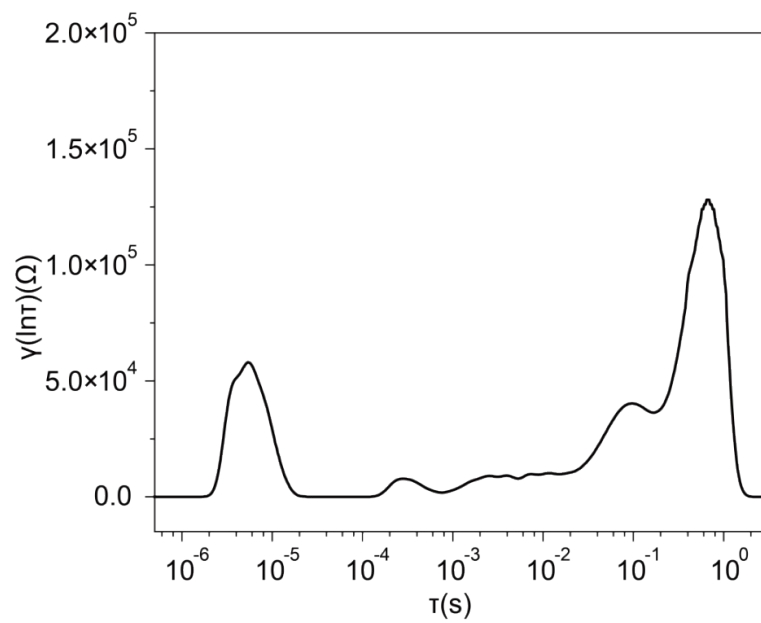


**Fig. S13.** DRT diagram of UiO-66-SO<sub>3</sub>H-1 at 60°C.

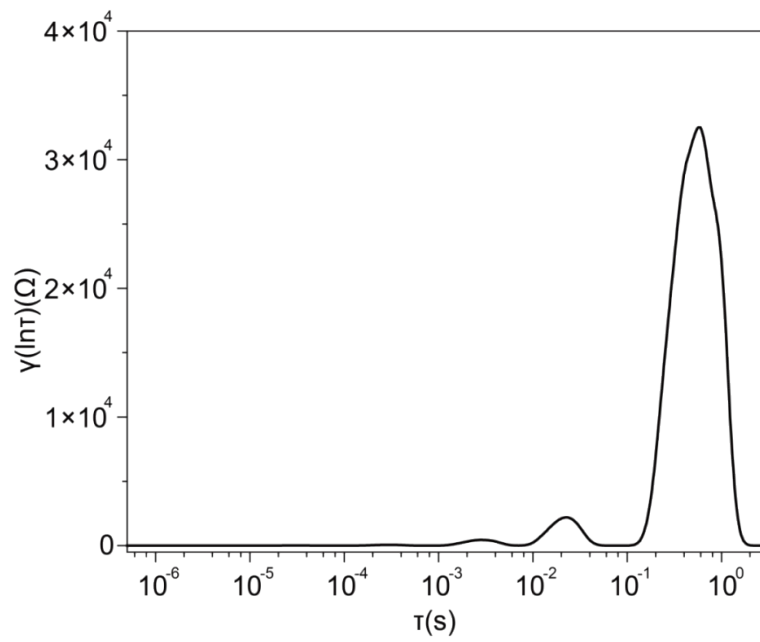


**Fig. S14.** DRT diagram of UiO-66-SO<sub>3</sub>H-2 at 60°C.

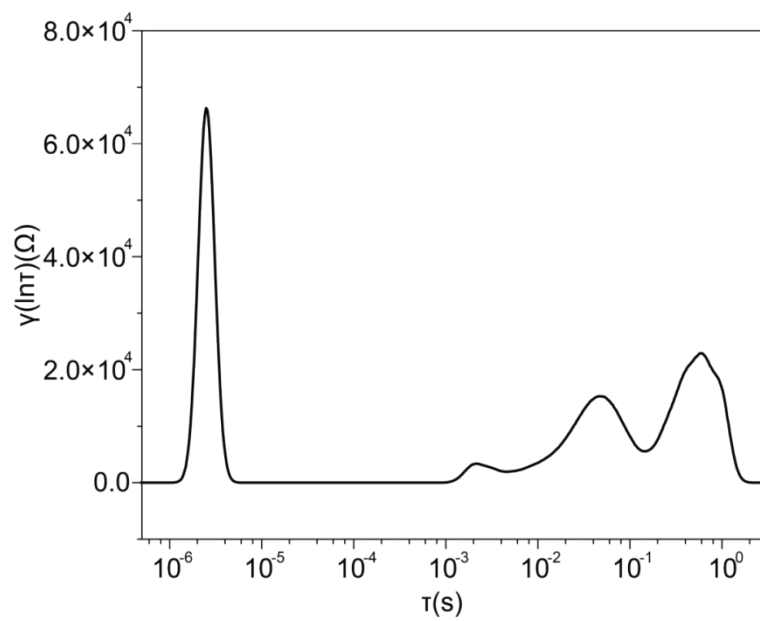


**Fig. S15.** DRT diagram of UiO-66-SO<sub>3</sub>H-1 at 70°C.

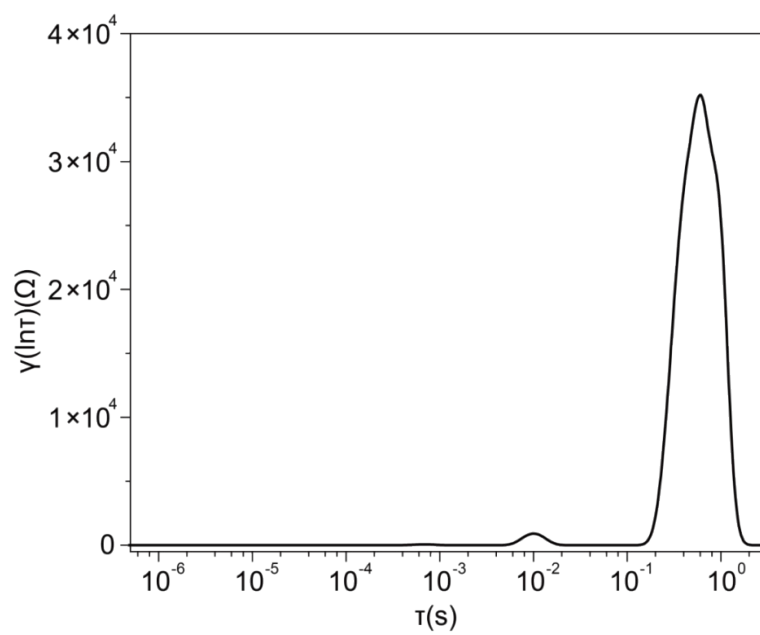


**Fig. S16.** DRT diagram of UiO-66-SO<sub>3</sub>H-2 at 70°C.

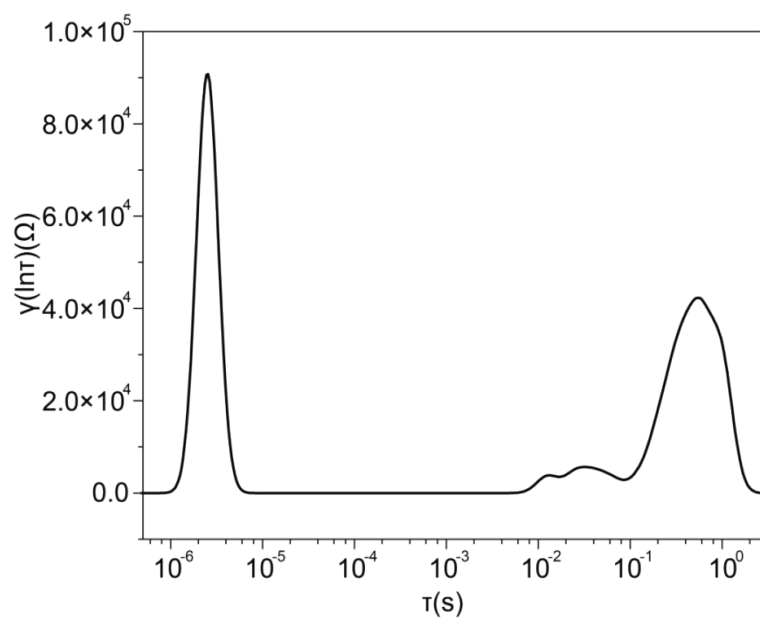


**Fig. S17.** DRT diagram of UiO-66-SO<sub>3</sub>H-1 at 80°C.

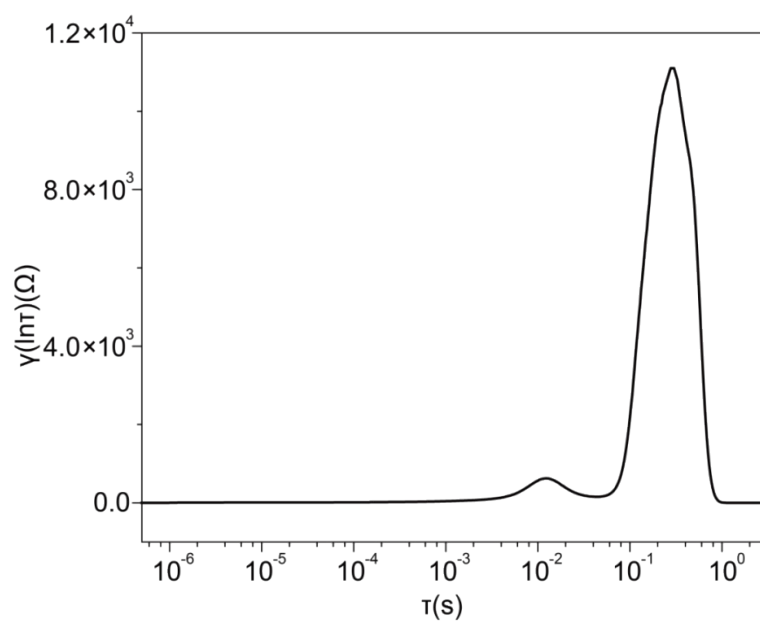


**Fig. S18.** DRT diagram of UiO-66-SO<sub>3</sub>H-2 at 80°C.

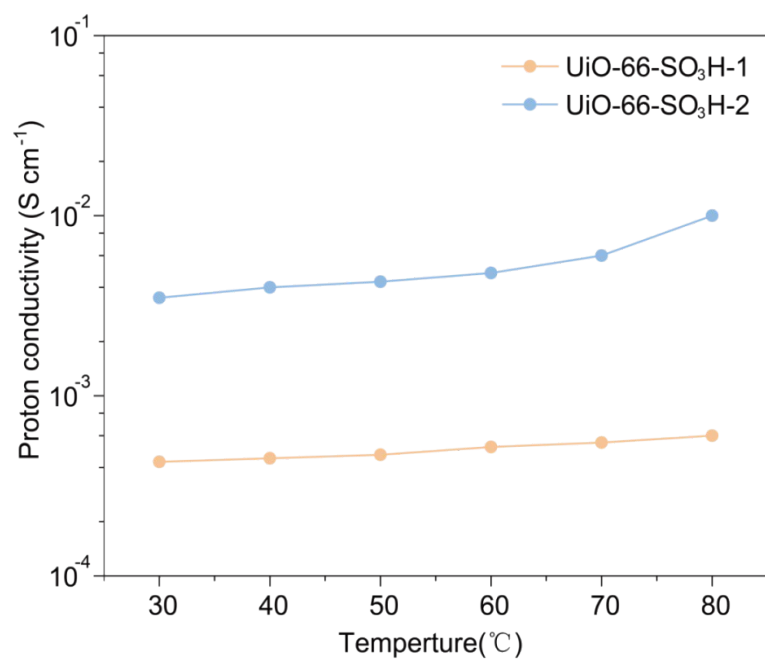


**Fig. S19.** Comparison of bulk proton conductivity among UiO-66-SO<sub>3</sub>H-1 and UiO-66-SO<sub>3</sub>H-2.

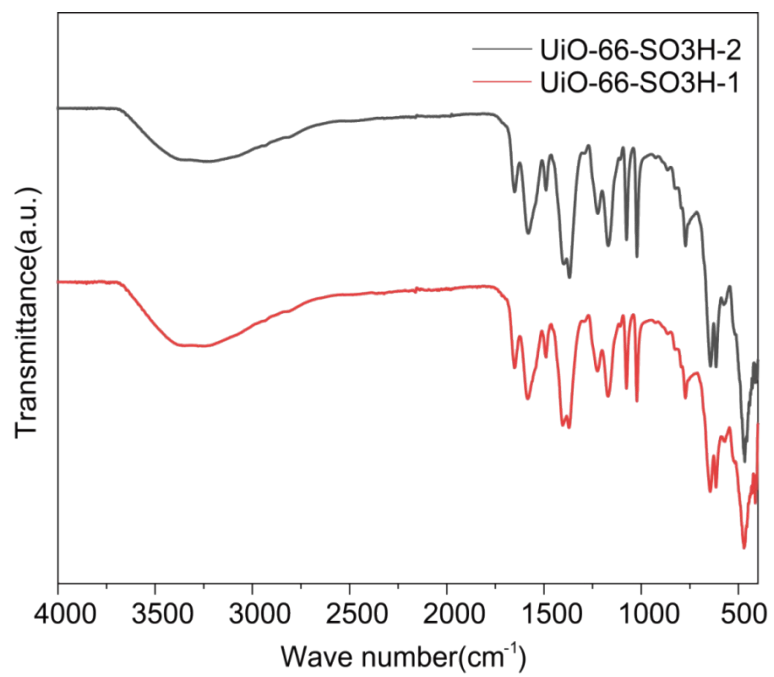


**Fig. S20.** FT-IR spectra of UiO-66-SO<sub>3</sub>H-1 and UiO-66-SO<sub>3</sub>H-2.

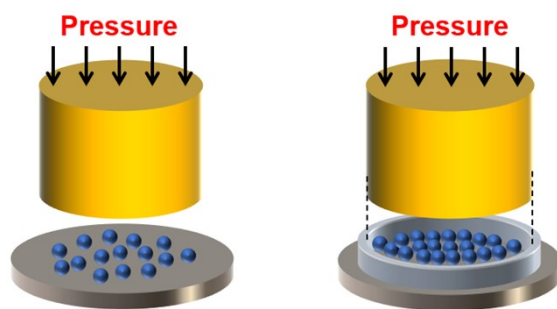


**Fig. S21.** Schematic comparison of the preparation protocols for UiO-66-SO<sub>3</sub>H-3 (left) and UiO-66-SO<sub>3</sub>H-2 (right).

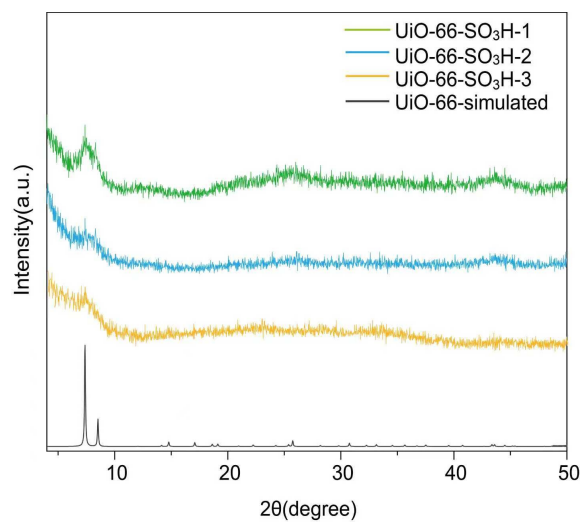


**Fig. S22.** PXRD of the three samples.

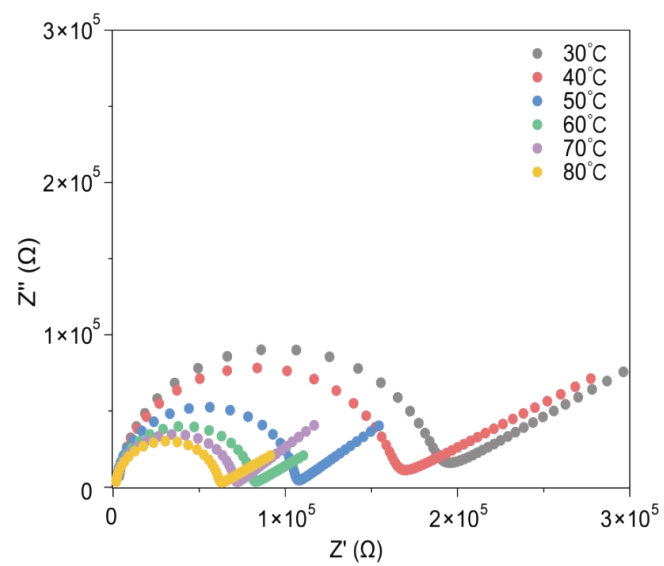


**Fig. S23.** Nyquist plot for UiO-66-SO<sub>3</sub>H-3 at 100% RH versus different temperatures.

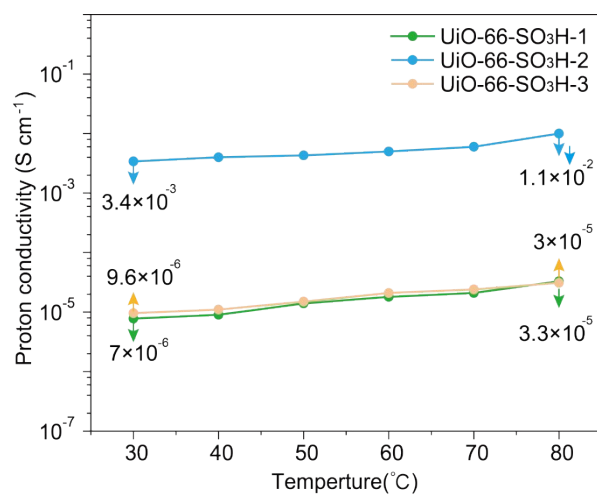


**Fig. S24.** Proton conductivity of the three samples.

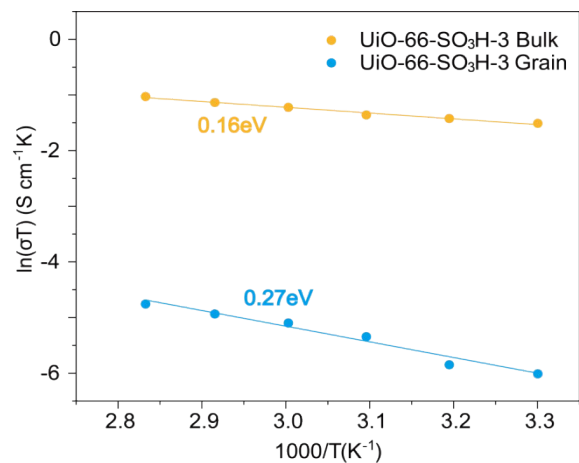


**Fig. S25.** Arrhenius plots of proton conductivity for UiO-66-SO<sub>3</sub>H-3 bulk and grain boundary part.

**Table 1.** Proton conductivity of other MOFs.

Compounds	Conductivity (S cm <sup>-1</sup> )	Conditions
UiO-66-SO <sub>3</sub> H-2	1.13×10 <sup>-2</sup>	T = 80°C, 100%RH
MIL-101-SO <sub>3</sub> H	1.16 × 10 <sup>-2</sup>	T = 80°C, 100%RH
CUST-861	2.96×10 <sup>-2</sup>	T =90°C, 98%RH
FDM-151	1.1×10 <sup>-2</sup>	T =95°C, 100%RH
MOF-bpe	1.95×10 <sup>-2</sup>	T=95 °C, 100% RH
MOF-bpy	2.6×10 <sup>-2</sup>	T=95 °C, 100% RH
MOP-1@DUT-68	7.58×10 <sup>-3</sup>	T=80 °C, 98% RH
MIP-202(Zr)	1.1×10 <sup>-2</sup>	T=90 °C, 95% RH
Im@MOF-808	3.45×10 <sup>-2</sup>	T=65°C, 98% RH
DUT-67(Zr)	2.98×10 <sup>-3</sup>	T=100°C, 98% RH
60-UiO-66-1.8	3×10 <sup>-2</sup>	T=100°C, 98% RH
ZrP-3	1.91×10 <sup>-2</sup>	T=90 °C, 95% RH
MOF-808-IMDC	1.11×10 <sup>-2</sup>	T=80°C, 98% RH
YCu161	1.84×10 <sup>-3</sup>	T=90°C, 98% RH
Cu-DSOA	1.9×10 <sup>-3</sup>	T=85°C, 98% RH
MOG-UiO-66	1.23×10 <sup>-2</sup>	T=80°C, 75% RH
MOG-MOF-808	3.06×10 <sup>-2</sup>	T=80°C, 75% RH
Nafion	8.0 × 10 <sup>-2</sup>	T = 80°C, 50%RH
Zr <sub>6</sub> O <sub>4</sub> (OH) <sub>8</sub> L <sub>4.2</sub> ·xH <sub>2</sub> O	1.93×10 <sup>-3</sup>	T=65°C, 95% RH

Table S2. The fitting parameters of the Nyquist plots of UiO-66-SO<sub>3</sub>H-1.

Tem(°C)	R1	R2	CPE1-T	CPE1-P	CPE2-T	CPE2-P
30	3295	178200	$2.540 \times 10^{-11}$	1.013	$3.522 \times 10^{-6}$	0.42821
40	3001	147370	$2.606 \times 10^{-11}$	1.011	$5.495 \times 10^{-6}$	0.56792
50	2807	93319	$9.468 \times 10^{-11}$	0.93674	$2.769 \times 10^{-6}$	0.87364
60	2682	73826	$1.159 \times 10^{-10}$	0.92414	$8.634 \times 10^{-6}$	0.33697
70	2600	63587	$2.499 \times 10^{-11}$	1.015	$3.896 \times 10^{-6}$	0.46375
80	2374	38168	$3.462 \times 10^{-11}$	0.99999	$4.137 \times 10^{-6}$	0.45731

Table S3. The fitting parameters of the Nyquist plots of UiO-66-SO<sub>3</sub>H-2.

Tem(°C)	R	CPE-T	CPE-P
30	114.3	$7.641 \times 10^{-6}$	0.83685
40	99.21	$1.735 \times 10^{-5}$	0.71624
50	93.15	$1.649 \times 10^{-5}$	0.78415
60	83.21	$1.002 \times 10^{-5}$	0.82544
70	68.82	$1.842 \times 10^{-5}$	0.81035
80	35.53	$8.434 \times 10^{-5}$	0.67573

Table S4. The fitting parameters of the Nyquist plots of UiO-66-SO<sub>3</sub>H-3.

Tem(°C)	R1	R2	CPE1-T	CPE1-P	CPE2-T	CPE2-P
30	1945	145280	$5.047 \times 10^{-11}$	0.99933	$2.6227 \times 10^{-6}$	0.3603
40	1840	123830	$2.772 \times 10^{-11}$	0.99349	$3.529 \times 10^{-6}$	0.33709
50	1783	96147	$5.105 \times 10^{-11}$	1.012	$7.043 \times 10^{-6}$	0.42861
60	1602	67228	$8.126 \times 10^{-10}$	0.89714	$9.121 \times 10^{-6}$	0.29087
70	1512	57664	$7.020 \times 10^{-11}$	1.009	$6.999 \times 10^{-6}$	0.44958
80	1400	45221	$9.483 \times 10^{-11}$	1.014	$1.338 \times 10^{-5}$	0.36942